Modeling the rupture process of the 2003 September 25 Tokachi-Oki (Hokkaido) earthquake using 1-Hz GPS data

Shin'ichi Miyazaki,[1,2] Kristine M. Larson,[3] Kyuhong Choi,[3] Kazuhito Hikima,[1] Kazuki Koketsu,[1] Paul Bodin,[4] Jennifer Haase,[5] Gordon Emore,[5] and Atsushi Yamagiwa[6]

Received 10 September 2004; accepted 3 October 2004; published 3 November 2004.

[1] High-rate GPS has the potential to recover both dynamic and static displacements accurately. We analyze 1-Hz GPS data recorded during the 2003 Tokachi-Oki earthquake. The 1-Hz GPS displacement waveforms show good agreement with integrated accelerometer records except for low frequency noise that are inherently present in integrated seismic records. The GPS waveforms were inverted to model the spatio-temporal evolution of the fault slip during the rupture. The slip is found to propagate downdip in the subduction zone with largest moment release ~50 km northwest of the hypocenter. The region of largest slip agrees in general with traditional seismic studies, indicating that 1-Hz GPS can be used for finite fault studies. The 1-Hz GPS slip model shows clearer contrast with afterslip distributions than those inferred from strong motion data, possibly because 1-Hz GPS is more sensitive to cumulative slip distribution. *INDEX TERMS:* 1294 Geodesy and Gravity: Instruments and techniques; 7209 Seismology: Earthquake dynamics and mechanics; 7212 Seismology: Earthquake ground motions and engineering. **Citation:** Miyazaki, S., K. M. Larson, K. Choi, K. Hikima, K. Koketsu, P. Bodin, J. Haase, G. Emore, and A. Yamagiwa (2004), Modeling the rupture process of the 2003 September 25 Tokachi-Oki (Hokkaido) earthquake using 1-Hz GPS data, *Geophys. Res. Lett.*, *31*, L21603, doi:10.1029/2004GL021457.

1. Introduction

[2] Seismic waveforms from various instruments and at different frequencies have been used to estimate the slip history of large earthquakes [*Olson and Apsel*, 1982; *Hartzell and Heaton*, 1983]. Teleseismic body waves retain relatively low frequencies and provide smoothed estimates that constrain the moment release rate and rupture orientation and size, but have less information about the "near-field terms" which include static offsets related to fault slip. Strong motion instruments (accelerometers) are used to constrain the detailed slip history, but their fidelity at recovering long period motions is limited both for reasons of instrument design and their inability to distinguish between linear accelerations and rotations [*Boore*, 2003]. GPS measurements are traditionally averaged over 24 hours to infer long-term (1–100 mm/yr) deformation rates, and hence, are usually limited to measuring the "static" or co-seismic displacements from an earthquake, and thus only serve to constrain the cumulative slip. Nevertheless, an accurate time-varying slip model should be able to fit both the seismic (dynamic) and geodetic (static) data with appropriate Green's functions [*Wald and Heaton*, 1994].

[3] Recently *Larson et al.* [2003] demonstrated that high sample-rate (1-Hz) GPS data could be analyzed with sufficient precision to measure seismic waves for the Denali Fault earthquake in Alaska. Due to the limited number of 1-Hz GPS stations, however, rupture models for that earthquake continue to be primarily constrained by seismic data. A geodetic instrument that accurately measure both the dynamic and static displacements would implicitly improve finite fault rupture studies by mitigating the tradeoff between rupture timing and slip location, an inherent limitation in waveform studies. For example, *Ji et al.* [2004] showed that 1-Hz GPS (horizontal) positions provided useful substitutes for seismometers in the sparsely-instrumented 2003 San Simeon earthquake.

[4] The advantage of 1-Hz GPS is that it is directly sensitive to displacement whereas strong motion instruments, which measure acceleration, must be integrated twice to obtain displacements, amplifying noise. The disadvantage of 1-Hz GPS is that it is many orders of magnitude less precise at high frequencies than a seismometer. To date, a time-varying fault slip model estimated from only 1-Hz GPS measurements has not been attempted. In this paper, we examine the capability of a 1-Hz GPS network to model the fault slip history of the Tokachi-Oki earthquake.

2. Observations

[5] The Tokachi-Oki earthquake occurred on 2003 September 25 at 19:50:07 UTC. The epicentral location was ~80 km offshore the northern island, Hokkaido (Figure 1). The rupture was close to the location of the 1952 Tokachi-Oki earthquake [*Yamanaka and Kikuchi*, 2003]. Peak ground accelerations of ~1g were observed at the coastal sites nearest the epicenter [*Honda et al.*, 2004], with resulting coseismic deformation exceeding 1 meter [*Miura et al.*, 2004]. Seismic moments for this event range from 0.8 to 3.5 $\times$ 10^{21} Nm, corresponding to Mw = 7.9–8.3 [*Honda et al.*, 2004].

[6] There is extensive geophysical instrumentation in Japan. The National Research Institute for Earth Science and Disaster Prevention (NIED) operates multiple (KiKnet,

[1]Earthquake Research Institute, University of Tokyo, Tokyo, Japan.
[2]Department of Geophysics, Stanford University, Stanford, California, USA.
[3]Department of Aerospace Engineering Sciences, University of Colorado, Boulder, Colorado, USA.
[4]CERI, University of Memphis, Memphis, Tennessee, USA.
[5]Department of Earth and Atmospheric Sciences, Purdue University, West Lafayette, Indiana, USA.
[6]Geographical Survey Institute, Tsukuba, Japan.

0094-8276/04/2004GL021457$05.00

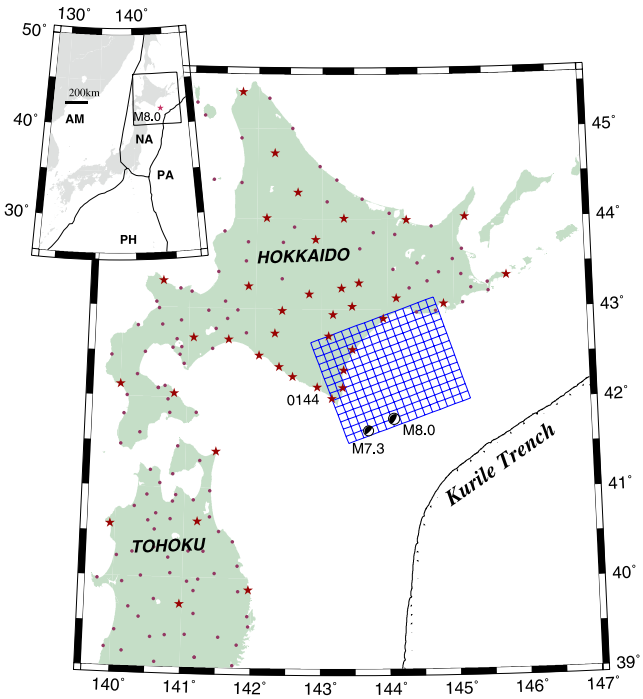

Figure 1. Location of the 2003 Tokachi-Oki earthquake epicenter, its largest aftershock, and the tectonic framework. 1-Hz GPS stations used in this study are shown as stars. Additional GEONET sites are shown by small circles. The fault plane used for the slip model is shown in blue.

Knet, Fnet) seismic networks [*Kinoshita*, 1998; *Aoi et al.*, 2000]; there are 185 Knet and 112 KiKnet accelerometer instruments on Hokkaido alone. Geodetic instrumentation in Japan is also widespread, with a 1000+ station GPS network, GEONET, operated by the Geographical Survey Institute (GSI). GEONET records and distributes GPS measurements at a 30-second sampling rate; it simultaneously operates many of these sites at 1-Hz. The high-rate data are telemetered in real-time for use in navigation and surveying. For the Tokachi-Oki earthquake, some of the 1-Hz GPS recordings were lost because the telemetry system lost power ~25 seconds into the event. Fortunately, very little 30-second data were lost and have been used in previous studies to estimate both the coseismic [*Miura et al.*, 2004] and postseismic [*Miyazaki et al.*, 2004] response to this earthquake.

[7] The 1-Hz GPS data were analyzed (Figure 1, Figure S1[1]) using the methods described in *Larson et al.* [2003]. Based on the standard deviation of GPS positions estimated for 500 seconds before the earthquake, the average precision of the east, north, and vertical 1-Hz GPS estimates is 4.5, 8.4, and 15.3 mm, respectively. Comparing the direct GPS observations with those inferred from seismic data highlights the strengths and weaknesses of the 1-Hz GPS data (Figure 2). At GEONET site 0144 (Figure 1) there are nearby KiKnet (HDKH07) and Knet (HKD110) strong motion sensors. While KiKnet also has borehole sensors, in this comparison we use the surface instrument because the GPS receiver and Knet instruments are also at the surface. The acceleration records were integrated after accounting for a baseline offset using the pre-event signal [*Boore*, 2003]. The horizontal position estimates for GPS and the KiKnet sensor compare well during the first ~50 seconds after the first arrival, after which low frequency noise in the seismic data causes the displacements to diverge significantly. There is excellent agreement throughout 150 seconds for the vertical component. The Knet recordings are significantly different than either GPS or KiKnet displacements although there is agreement at high frequencies. The discrepancies could be due to errors introduced by integrating the noisy signal, by tilting at the site, or by sensor orientation error.

3. Model Description

[8] The 1-Hz GPS data for 37 stations (Figure S1) were inverted to infer temporal history of the rupture on the plate interface using the multiple time-window method [*Olson and Apsel*, 1982; *Yoshida et al.*, 1996]. As our initial estimate of the fault plane geometry, we used the results of *Yagi* [2004], who inverted teleseismic and strong motion data for this earthquake. We adopted his hypocentral location 41.78°N, 144.08°E, and fault orientation strike (250°) and dip (20°). A hypocentral depth of 25 km was adopted to match the iso-depth contours of the Kurile Trench [*Katsumata et al.*, 2003]. The fault geometry is defined to be 160 km long and 140 km, divided into 10 by 10 km fault segments with rake angle of 105 degrees (Figure 1).

[9] Recent development of methods to calculate both dynamic and static displacement responses enables us to directly invert displacement waveforms for the rupture estimation. We used the frequency-wavenumber method of *Zhu and Rivera* [2002] to calculate theoretical Green's functions, assuming the velocity structure shown in Table S1. Unlike synthetics produced by the reflectivity method [*Kohketsu*, 1985], the Green's functions we used can faithfully reproduce both dynamic and static displacement components including the near-field terms. Ramp functions with a rise time of 2 seconds were used as the

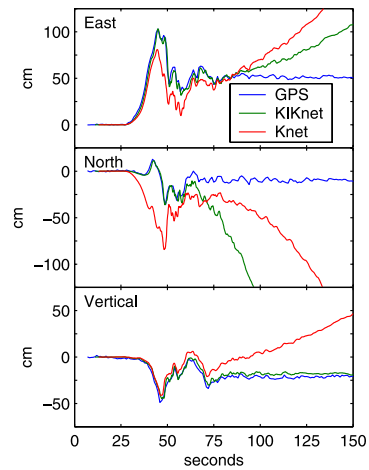

Figure 2. Comparison of 1-Hz GPS (blue-0144) and integrated acceleration records for KiKnet (green-HDKH07) and Knet (red-HKD110).

[1]Auxiliary material is available at ftp://ftp.agu.org/apend/gl/2004GL021457.

temporal basis functions, with 10 basis functions (time windows) at each fault segment. We filtered both the observations and the Green's functions with a 0.25 Hz low-pass filter, to be consistent with the resolution of our fault parameterization. We assumed the rupture started from the hypocenter and the first time window propagated with a velocity of 4.4 km/s (3.4 km/s for the northeast segments) which we obtained by maximizing the likelihood function.

[10] We assumed the observation errors were a combination of the measurement precision given previously and the accuracy of the forward modeling parameterization. We approximated the latter to be proportional to the maximum amplitudes of the displacements. Each observation in the inversion was weighted by the inverse of the combined standard deviation, given as the square root of the sum of the variances of the measurement error and parameterization error. A positivity constraint was imposed so that the rake angle of slip is within $105° \pm 45°$. A smoothness constraint in space and time was used to stabilize the inversion [*Akaike*, 1980].

4. Results and Discussion

[11] Figure 3 summarizes the results of the 1-Hz GPS fault slip inversion, with both total slip and time-varying estimates of slip-rate. The fit between the observations and synthetic displacements is consistent with the assigned observation errors (Figure S2), and the normalized root mean square for the data is 1.08. There is more complexity in the GPS observations than the synthetics at many of the sites. For example, GPS station 0521 is located in the middle of a large basin on the banks of the Tokachi River. There is a 4 second resonance observed strongly at this station that is likely a basin wave (J. Clinton, personal communication, 2004).

[12] The rupture propagated downdip to the northwest, with the largest slip concentrated ~50 km from the hypocenter, reaching a total of ~9 meters (Figure S3). A secondary slip maximum, possibly triggered by the initial slip, was found in the northeast segment (total slip of 2 meters). We compute a cumulative moment of 1.8×10^{21} Nm, which corresponds to $M_W \sim 8.1$. Note also that the largest aftershock ($M \sim 7.1$) occurred in the southwest side of the fault plane, where we estimate no significant coseismic slip.

[13] How well does our slip model agree with other published slip models? These kinds of comparisons are difficult because each study uses a different station distribution, parameterization and procedures. Four slip models based on seismic data were recently published: *Yamanaka and Kikuchi* [2003] used 25 teleseismic records; *Yagi* [2004] combined 12 teleseismic stations with 12 surface strong motion sites on Hokkaido; *Honda et al.* [2004] used 15 surface strong motion sites; and *Koketsu et al.* [2004] used 11 strong motion borehole instruments on Hokkaido and static GPS displacements. All four seismic models and our seismo-geodetic study find a large area of slip northwest of the epicenter, although the location of the maximum slip region varies by as much as ~20 km among the five models. Cumulative slip distributions are different among those four studies: *Yamanaka and Kikuchi* [2003] found a relatively large single slip locus. *Yagi* [2004] found that the rupture occurred at 3 asperities. *Koketsu et al.* [2004] inferred a single large asperity; *Honda et al.* [2004] found two major loci to the northwest of the epicenter, one minor locus near the epicenter, with one minor locus at the northeast edge of the fault. Our coseismic slip model makes a clear contrast with afterslip (Figure 3a) estimated for the following 30 days [*Miyazaki et al.*, 2004]. The larger slip patch is located where neither significant afterslip nor aftershocks [*Ito et al.*, 2004] were observed; the region of smaller slip is located at the deeper edge of the afterslip. On the other hand, seismic waveform inversion studies [*Honda et al.*, 2004; *Yagi*, 2004] find a maximum downdip where more than 20 cm of afterslip was observed. We suggest that almost all of the accumulated stress was released by high-speed rupture in "asperities" [*Yamanaka and Kikuchi*, 2004], and that afterslip and some aftershocks were concentrated in the surrounding regions due to stress transfer.

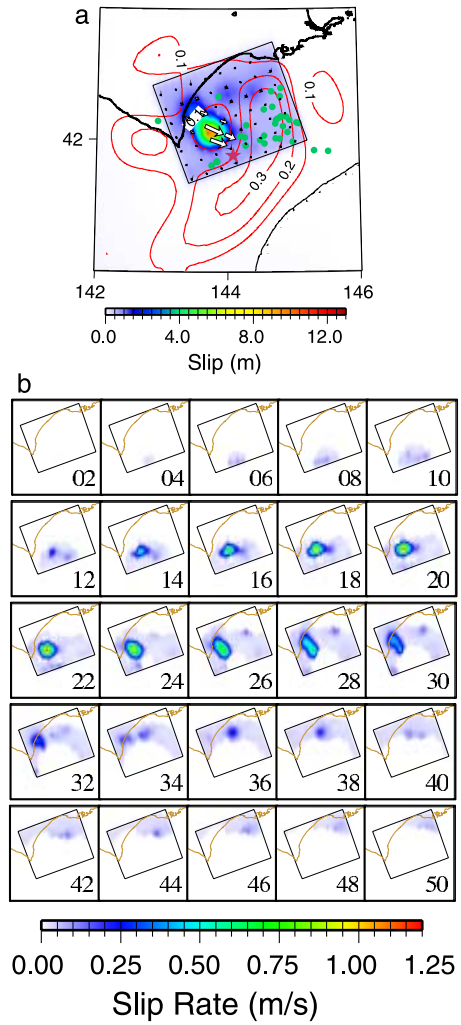

Figure 3. 1-Hz GPS model results for a) cumulative slip and b) slip-rate as a function of time (seconds given in lower right corner). Epicenter location shown as a star. Arrows are slip vectors, with length indicating the amount of slip and the direction indicates the rake angle. Aftershocks greater than magnitude 4 are shown as green circles [*Ito et al.*, 2004]. Red contours show postseismic deformation in meters [*Miyazaki et al.*, 2004].

Since 1-Hz GPS gives a stronger constraint on (cumulative) slip distributions, our model shows more consistency with afterslip.

[14] We also found significant slip in the northeast area of the fault plane, as inferred by *Yamanaka and Kikuchi* [2003] and *Honda et al.* [2004] but not by *Yagi* [2004]. *Koketsu et al.* [2004] show a smooth broad slip distribution centered near our highest slip but lacking any clear slip locus in the northeast region of the fault. Unlike *Yagi* [2004] and *Honda et al.* [2004], we found no significant slip around the hypocentral region. It has been suggested that offshore seismic data provide a better constraint on slip in this region than the seismic and geodetic networks installed on land (C. Ji, personal communication, 2004).

[15] There are also two estimates of total fault slip from static GPS measurements [*Miura et al.*, 2004; *Koketsu et al.*, 2004]. In each estimate the region of large slip had similar slip amplitude to seismic studies but was ~20 km closer to the hypocenter than estimated with seismic waveforms. These geodetic studies used an elastic half-space in their models. However, crustal complexity will degrade the accuracy of using a half-space approximation for calculating geodetic Green's functions [*Wald and Graves*, 2001]. For example, *Savage* [1998] showed that use of an elastic half-space Green's function tends to locate the slip in shallower regions. The discrepancy between the geodetic and seismic slip estimates may also reflect the difficulty of isolating coseismic displacements from daily GPS time series. In the future we will invert the three data sets (teleseismic, seismic strong motion, and 1-Hz GPS strong motion) separately using common fault model parameterizations. This will help determine which features in the slip model are best constrained by each dataset.

5. Concluding Remarks

[16] These results demonstrate that a 1-Hz GPS network in the near-field can accurately recover slip histories of large earthquakes. This suggests that existing and future GPS instrumentation should be operated simultaneously at low and high sampling rates. The low sample rate GPS data measures long-term deformation. The high-rate GPS data can be downloaded if a seismic event occurs. This kind of mixed-mode sampling rate has been proposed for NSF-Earthscope which is in the process of installing 1000+ GPS receivers throughout the western United States.

[17] **Acknowledgments.** S. M. was supported by a JSPS fellowship for research abroad. NSF supported this research by grants to CU (EAR-0337206), Memphis (EAR-0337108), and Purdue (EAR-0337549). GSI operates GEONET. JPL, IGS, and UNAVCO provided infrastructure support. Comments from R. Burgmann, K. Hirahara, J. Savage, A. Venkataraman and D. Wald significantly improved the manuscript. We thank L. Zhu and R. Graves for providing their FK code to us.

References

Akaike, H. (1980), Likelihood and Bayes procedure, in *Bayesian Statistics*, edited by J. M. Bernardo et al., pp. 143–166, Univ. Press, Valencia, Spain.

Aoi, S., K. Obara, S. Hori, K. Kasahara, and Y. Okada (2000), New strong-motion observation network: KiK-net, *Eos Trans. AGU*, *81*(48), Fall Meet. Suppl., Abstract S71A-05.

Boore, D. M. (2003), Analog-to-digital conversion as a source of drifts in displacements derived from digital recordings of ground acceleration, *Bull. Seismol. Soc. Am.*, *93*, 2017–2024.

Hartzell, S., and T. H. Heaton (1983), Inversion of strong ground motion and teleseismic waveform data for the fault rupture history of the 1979 Imperial Valley, California earthquake, *Bull. Seismol. Soc. Am.*, *73*, 1553–1583.

Honda, R., S. Aoi, N. Morikawa et al. (2004), Ground motion and rupture process of the 2003 Tokachi-oki earthquake obtained from strong motion data of K-NET and KiK-net, *Earth Planets Space*, *56*, 317–322.

Ito, Y., H. Matsubayashi, H. Kimura et al. (2004), Spatial distribution for moment tensor solutions of the 2003 Tokachi-oki earthquake (M = 8.0) and aftershocks, *Earth Planets Space*, *56*, 301–306.

Ji, C., K. Larson, Y. Tan et al. (2004), Slip history of the 2003 San Simeon Earthquake constrained by combining 1-Hz GPS, strong motion, and teleseismic data, *Geophys. Res. Lett.*, *31*, L17608, doi:10.1029/2004GL020448.

Katsumata, K., N. Wada, and M. Kasahara (2003), Newly imaged shape of the deep seismic zone within the subducting Pacific plate beneath the Hokkaido corner, Japan-Kurile arc-arc junction, *J. Geophys. Res.*, *108*(B12), 2565, doi:10.1029/2002JB002175.

Kinoshita, S. (1998), Kyoshin net (k-net), *Seismol. Res. Lett.*, *69*, 309–332.

Kohketsu, K. (1985), The extended reflectivity method for synthetic near-field seismograms, *J. Phys. Earth*, *33*, 121–131.

Koketsu, K., K. Hikima, S. Miyazaki, and S. Ide (2004), Joint inversion of strong motion and geodetic data for the source process of the 2003 Tokachi-oki, Hokkaido, earthquake, *Earth Planets Space*, *56*, 329–334.

Larson, K. M., P. Bodin, and J. Gomberg (2003), Using 1-Hz GPS data to measure deformations caused by the Denali fault earthquake, *Science*, *300*, 1421–1424.

Miura, S., Y. Suwa, A. Hasegawa, and T. Nishimura (2004), The 2003 M8.0 Tokachi-Oki earthquake: How much has the great event paid back slip debts?, *Geophys. Res. Lett.*, *31*, L05613, doi:10.1029/2003GL019021.

Miyazaki, S., P. Segall, J. Fukuda, and T. Kato (2004), Space-time distribution of afterslip following the 2003 Tokachi-oki earthquake: Implications for variations in fault zone frictional properties, *Geophys. Res. Lett.*, *31*, L06623, doi:10.1029/2003GL019410.

Olson, A. H., and R. J. Apsel (1982), Finite faults and inverse-theory with applications to the 1979 Imperial-Valley earthquake, *Bull. Seismol. Soc. Am.*, *72*, 1969–2001.

Savage, J. C. (1998), Displacement field for an edge dislocation in a layered half-space, *J. Geophys. Res.*, *103*, 2439–2446.

Wald, D. J., and R. W. Graves (2001), Resolution analysis of finite fault source inversion using one- and three-dimensional Green's functions: 2. Combining seismic and geodetic data, *J. Geophys. Res.*, *106*, 8767–8788.

Wald, D. J., and T. H. Heaton (1994), Spatial and temporal distribution of slip for the 1992 Landers, California, earthquake, *Bull. Seismol. Soc. Am.*, *84*, 668–691.

Yagi, Y. (2004), Source rupture process of the 2003 Tokachi-oki earthquake determined by joint inversion of teleseismic body wave and strong ground motion data, *Earth Planets Space*, *56*, 311–316.

Yamanaka, Y., and M. Kikuchi (2003), Source processes of the recurrent Tokachioki earthquake on September 26, 2003, inferred from teleseismic body waves, *Earth Planets Space*, *55*, 21–24.

Yamanaka, Y., and M. Kikuchi (2004), Asperity map along the subduction zone in northeastern Japan inferred from regional seismic data, *J. Geophys. Res.*, *109*, B07307, doi:10.1029/2003JB002683.

Yoshida, S., K. Koketsu, B. Shibazaki et al. (1996), Joint inversion of near- and far- field waveforms and geodetic data for the rupture process of the 1995 Kobe earthquake, *J. Phys. Earth*, *44*, 437–454.

Zhu, L., and L. A. Rivera (2002), A note on the dynamic and static displacements from a point source in multilayered media, *Geophys. J. Int.*, *148*, 619–627.

P. Bodin, CERI, University of Memphis, Memphis, TN 38152, USA.

K. Choi and K. Larson, Department of Aerospace Engineering Sciences, UCB 429, University of Colorado, Boulder, CO 80309, USA. (kristine.larson@colorado.edu)

G. Emore and J. Haase, Department of Earth and Atmospheric Sciences, Purdue University, West Lafayette, IN 47907, USA.

K. Hikima and K. Koketsu, Earthquake Research Institute, University of Tokyo, Tokyo, 113-0032, Japan.

S. Miyazaki, Department of Geophysics, Stanford University, Stanford, CA 94305, USA.

A. Yamagiwa, Geographical Survey Institute, Tsukuba, 305-0032, Japan.